Fermi National Accelerator Laboratory

FERMILAB Conf-96/210-E
CDF

W/Z at CDF

R.M. Thurman-Keup
For the CDF Collaboration

Department of Physics
The University of Illinois
1110 West Green Street, Urbana, Illinois 61801

Fermi National Accelerator Laboratory
P.O. Box 500, Batavia, Illinois 60510-0500

August 1996

Published Proceedings of the *XIth Topical Workshop on $p\bar{p}$ Collider Physics,* Padova, Italy, May 27-June 1, 1996.

Disclaimer

CDF/PUB/ELECTROWEAK/PUBLIC/3765

W/Z AT CDF

R. M. THURMAN-KEUP[a]
Department of Physics, University of Illinois, 1110 West Green Street, Urbana, IL 61801, USA

Results are presented based on 19pb^{-1} of data collected by the CDF detector during the 1992-1993 collider run at the Fermilab Tevatron. These results include measurements of the W mass and $\sigma \cdot B$ for W and Z decays using both the electron and muon channels. In addition to extracting the total width of the W using the ratio of cross sections, a direct measurement of the W width using the electron decay channel is also presented.

1 Introduction

During the 1992-1993 collider run at the Fermilab Tevatron, CDF recorded $\bar{p}p$ collisions corresponding to an integrated luminosity of 19pb^{-1}. Out of this data, roughly 20,000 W decays (combined electron and muon channels), and some 1700 Z decays were extracted. With these W and Z events, a variety of electroweak measurements are made including presented in this paper: the production cross sections,[1] and the W mass,[2] and width.[3] Since descriptions of the CDF detector abound in the literature.[4] there will be none presented here.

2 W and Z Cross Sections and W Width

The ratio $R = \sigma \cdot B(W \rightarrow \ell\nu)/\sigma \cdot B(Z \rightarrow \ell\ell)$ is related to the width of the W by $\Gamma_W = \frac{\Gamma(W\rightarrow\ell\nu)\cdot\sigma_W/\sigma_Z}{B(Z\rightarrow\ell\ell)} \times \frac{1}{R}$. Using theoretical values for the ratio σ_W/σ_Z and for $\Gamma(W \rightarrow \ell\nu)$, LEP measurements for $B(Z \rightarrow \ell\ell)$, and R from above, one can obtain the total width of the W. This measurement is sensitive to non-standard model decays of the W or when compared with direct measurements of the W width provides another consistency check of the standard model.

2.1 Event Selection

Events containing a W or Z are characterized by at least one high transverse momentum ($p_T > 20\ GeV$) lepton with pseudorapidity, $|\eta| < 1.0$. In addition, W events have missing transverse energy, $\not\!\!E_T$, characteristic of neutrinos, and Z events have another high-p_T lepton with a larger allowed η range. Missing

[a]representing the CDF collaboration

Table 1: The measured cross section times branching ratios for both $W \to \ell\nu$ and $Z \to \ell\ell$ processes along with the ratio, R of $W \to \ell\nu$ to $Z \to \ell\ell$.

	$W \to \ell\nu$	$Z \to \ell\ell$
$(\sigma \cdot B)_e$	$2.49 \pm 0.08 \pm 0.09(lum)$ nb	$0.231 \pm 0.009 \pm 0.008(lum)$ nb
R_e	10.90 ± 0.43	

energy is a vector sum defined as $\not\!\!E_T = |\vec{\not\!\!E}_T| = -\sum E_i \sin\theta_i \hat{\mathbf{n}}_i - \vec{p}_T^{\,\ell}$, where E_i, θ_i, and $\hat{\mathbf{n}}_i$ are the energy of, polar angle of, and transverse unit vector to the i^{th} calorimeter tower. The energy in the towers is measured after removing the lepton contribution.

2.2 Cross Sections and Width

The measured values for the cross sections times branching ratios and the ratio R are listed in Table 1. The theoretical curves of $\sigma \cdot B$ as functions of $\sqrt{s}$ are plotted in Fig. 1a along with the experimental points. The agreement between theory and experiment is exceptional when compared to other various QCD tests. Using the values in Table 1 for R, the total width of the W for the electron channel is

$$\Gamma_W^e = 2.043 \pm 0.082 \text{ GeV} \tag{1}$$

when the standard model predicts $\Gamma_W^{\rm SM} = 2.077 \pm 0.014$ GeV. These and other width results are summarized in Fig. 1b.

A direct measurement of the width is also possible by using the high transverse mass tail of the W spectrum. Here, detector resolutions are decreasing in a gaussian fashion whereas the lineshape is only falling as a power law. The advantage to this method other than being a direct measurement, is that it is not dominated by systematics. The transverse mass tail above 110 GeV/c^2 (Fig. 1c) is compared to Monte Carlo simulations at various W widths and a likelihood fit is used to determine the best width value. The fit value of

$$\Gamma_W^e(direct) = 2.11 \pm 0.28(stat) \pm 0.16(syst) \text{ GeV} \tag{2}$$

is consistent with both the indirect method and the standard model.

3 *W* Mass

The mass of the W, M_W, is an important parameter of the standard model because of its sensitivity to radiative corrections in the theory. These corrections

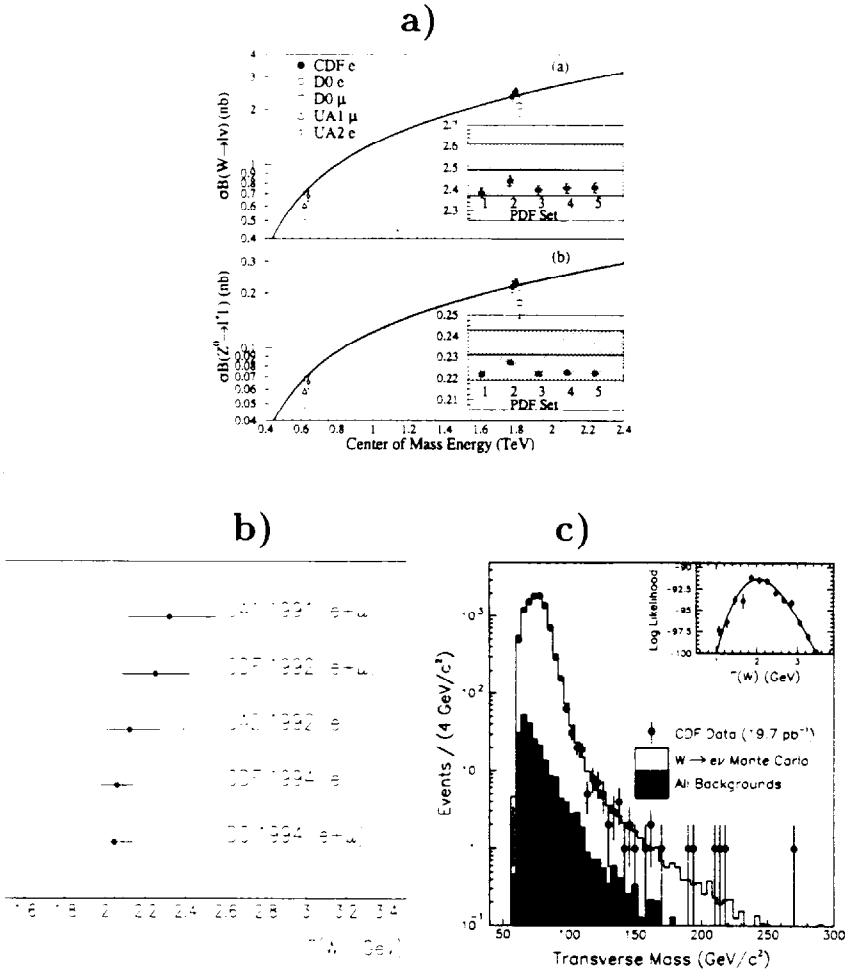

Figure 1: a) Plots of $\sigma \cdot B$ for $W \to \ell\nu$ and $Z \to \ell\ell$. b) Indirect measurements of the W width using the relationship between R and Γ_W. c) Direct measurement of Γ_W from the tail of the W transverse mass spectrum. The fitted value is 2.11 ± 0.32 GeV.

produce dependencies between M_W and other standard model parameters such as the mass of the top quark and the mass of the higgs boson. A precision measurement of M_W not only tests the consistency of the standard model, but can provide a weak constraint on the mass of the as yet undiscovered higgs.

3.1 Event Selection

Several data sets in addition to $W \rightarrow e\nu$ and $W \rightarrow \mu\nu$ are utilized in the measurement of M_W. The absolute momentum scale is extracted from a sample of $J/\psi \rightarrow \mu\mu$ decays and is checked with both $\Upsilon \rightarrow \mu\mu$ and $Z \rightarrow \mu\mu$ samples, the latter of which also determines the momentum resolution. An inclusive electron data sample is used to perform a relative calibration of the central electromagnetic calorimeter. The absolute energy scale is obtained from $W \rightarrow e\nu$ events and checked with $Z \rightarrow ee$ events which are also used in determining the energy resolution.

Event selection for the W and Z data sets involves most of the criteria discussed above for generic W and Z events, while adding a number of restrictions intended to clean up the event sample. The lepton energy cuts are increased to 25 GeV to reduce the backgrounds which exhibit a typical falling spectrum. The transverse momentum of the W as measured by the calorimeter is required to be less than 20 GeV and no jet is allowed to be greater than 30 GeV. These two cuts reduce the energy present in the calorimeter and result in better energy resolution for the neutrino. The transverse mass of the lepton and neutrino must be between 65 GeV/c^2 and 100 GeV/c^2, further eliminating backgrounds present at lower energies.

3.2 Momentum Calibration

The momentum calibration proceeds in three steps: the alignment of the tracking chamber (CTC), the absolute momentum scale calibration, and a determination of the momentum resolution.

The alignment of the tracking chamber is accomplished using a sample of electrons with $p_T > 18$ GeV. The alignment requires the average E/p [b] of electrons and positrons to be equal taking advantage of the fact that the calorimeter, to a high degree of precision, cannot tell the difference between e^+ and e^-. There is a residual misalignment to the CTC in η which because of the charge asymmetry of W decays produces a 15 MeV/c^2 uncertainty in M_W.

[b] The quantity E/p is the ratio of an electron/positron's energy measured in the calorimeter to its momentum measured in the tracking chamber.

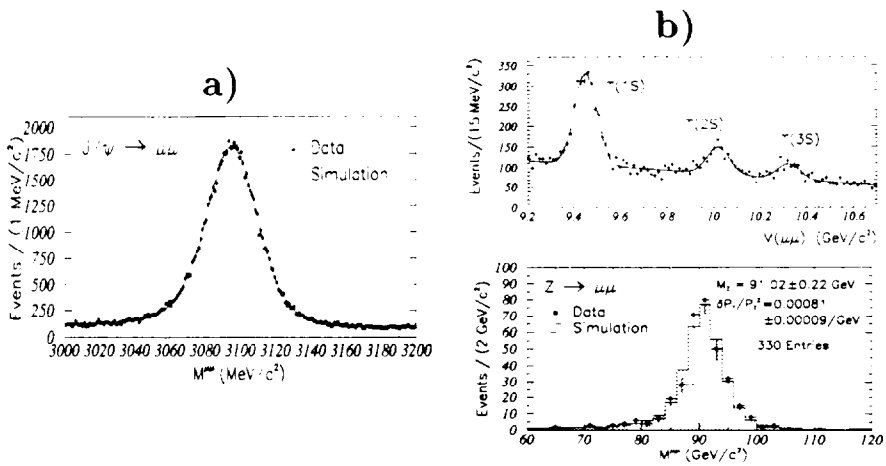

Figure 2: a) Invariant mass distribution of $J/\psi \rightarrow \mu\mu$ events. The curve is a radiative Monte Carlo simulation. b) The top is the invariant mass distribution of muon pairs in the vicinity of the Υ resonance. The first three radial states can be clearly seen. The bottom is the mass distribution of $Z \rightarrow \mu\mu$ events from which the momentum resolution is extracted.

The momentum scale calibration is accomplished using approximately 60.000 $J/\psi \rightarrow \mu\mu$ (Fig. 2a) decays with which the mass of the J/ψ is measured and compared with the world average. The fitted J/ψ mass is 3097.3 ± 1.8 MeV/c^2 compared to the world average of 3096.88 ± 0.04 MeV/c^2 resulting in a momentum scale of 0.99984 ± 0.00058. The uncertainties in determining the momentum scale are listed in Table 2.

Statistical — The mass is extracted from a gaussian plus linear background fit in a ± 50 MeV/c^2 window around the peak.

Background — The uncertainty due to the background shape is estimated by fitting the background with several functional forms.

Muon Energy Loss — The muons lose energy in the material between the beamline and the tracking chamber. The amount of material is determined from the radiative tail of E/p and the type of material is obtained from a priori accounting. The amount of material is checked using $\gamma \rightarrow e^+e^-$ conversions. In the current collider run, photon conversions will be used as the primary material estimate.

Beam Constraint, etc. — A significant fraction of J/ψ s originate from b quark decays which occur some distance from the beamline. Constraining the muons to have originated from the beamline introduces a systematic uncertainty. Uncertainties in the knowledge of the magnetic field and a small unexplained time

Table 2: a) Uncertainties in the momentum scale calibration. The subtotal reflects the uncertainty in just the J/ψ mass determination and the total includes the extrapolation to the momentum regime of W decays. b) Uncertainties in the energy scale calibration. The subtotal reflects the uncertainty in just the energy scale determination and the total includes the uncertainty in the momentum scale which enters through the p in E/p.

a) Momentum Scale Uncertainty	$\delta M_{J/\psi}$ MeV/c^2
Statistical	0.1
Background	0.1
Muon Energy Loss	1.3
Beam Constraint, Field Non-uniformity, Time Variation	0.8
Radiative Decay	0.2
Subtotal	**1.6**
Extrapolation to M_W	0.9
Total	**1.8**

b) Energy Scale Uncertainty	δM_W MeV/c^2
Statistical	65
Material Scale	70
Electron Resolution	50
Fitting	15
Subtotal	**110**
Momentum Scale	50
Total	**120**

variation in the $J/\psi \rightarrow \mu\mu$ peak also contribute.

Radiative Decay — The mass is obtained from a gaussian fit forcing the need to correct for the asymmetric radiative tail of the resonance. This correction is determined from a radiative monte carlo.

Extrapolation to M_W — Using the J/ψ peak fixes the momentum scale at the J/ψ mass; however, nonlinearities in the tracking chamber measurement may add an uncertainty to the momentum scale at the W mass. Since the tracking chamber measures positions, the figure of merit for extrapolating is curvature, $c = 1/p_T$. The curvature lever arm provided by the J/ψ sample is much longer than the extrapolation distance to M_W thus ensuring a relatively small uncertainty which has been expressed as an uncertainty in the J/ψ mass. The total uncertainty of 1.8 MeV/c^2 corresponds to an uncertainty in M_W of 50 MeV/c^2. The momentum scale has been check using $\Upsilon \rightarrow \mu\mu$ and $Z \rightarrow \mu\mu$ decays (Fig. 2b). The fitted values agree with the world averages as shown in Table 3.

The momentum resolution is extracted from the width of the $Z \rightarrow \mu\mu$ peak and is parameterized as $\delta p_T/p_T = k \cdot p_T$ where the constant is found to be 0.00081 ± 0.00009 (GeV/c)$^{-1}$. The uncertainty in the momentum resolution translates into a 60 MeV/c^2 uncertainty in M_W.

Table 3: Table of fitted mass values for the $\Upsilon \rightarrow \mu\mu$ and $Z \rightarrow \mu\mu$ resonances together with the world averages. The second uncertainty is the momentum scale uncertainty.

$\mu\mu$ Resonance	Measured Mass (MeV/c^2)	PDG Mass [5] (MeV/c^2)
Υ(1s)	$9460 \pm 2 \pm 5$	9460.3 ± 0.2
Υ(2s)	$10029 \pm 5 \pm 5$	10023.3 ± 0.3
Υ(3s)	$10334 \pm 8 \pm 6$	10355.3 ± 0.5
Z	$91020 \pm 210 \pm 55$	91187 ± 7

3.3 Energy Calibration

The energy calibration consists of a relative calorimeter tower calibration, an absolute scale calibration and a determination of the energy resolution.

The relative calibration is accomplished using $\sim$ 140,000 low energy electrons ($E_T > 8$ GeV) and requiring the average E/p to be the same in all calorimeter towers and to be uniform within a tower. This results in a flat calorimeter response and better energy resolution.

The absolute energy scale is derived from the momentum scale by again using E/p from $W \rightarrow e\nu$ events (Fig. 3a). The energy scale is adjusted such the data agree with a radiative Monte Carlo including both internal and external bremsstrahlung. The uncertainties in the energy scale, expressed as uncertainties in M_W. are discussed below and listed in Table 2.

Statistical — The E/p distribution is fit to a Monte Carlo radiative simulation in the region $0.9 < E/p < 1.1$ and the energy scale is extracted from that fit.

Material Scale — As stated earlier, the amount of material is extracted from the radiative tail of E/p. The material in the simulation is adjusted to produce the best fit in the region $1.3 < E/p < 2.0$. The amount of material is found to be $(8.9 \pm 0.9)\%$ of a radiation length. This amount is checked using photon conversions which give a result of $(8.1 \pm 0.4)\%X_0$ (Fig. 3c).

Electron Resolution — Any uncertainty in the electron resolution translates to a systematic uncertainty in the mean of E/p since the E/p distribution is not symmetric.

Fitting — The fit to E/p is performed exactly the same as the fit for the W mass and thus contributes an uncertainty.

A total uncertainty of 120 MeV/c^2 is accumulated after including the momentum scale uncertainty. The energy scale is checked using $Z \rightarrow ee$ events and the fitted mass agrees with the world average of 91.187 ± 0.007 GeV/c^2 (Fig. 3b).

As with the momentum resolution, the energy resolution is extracted from

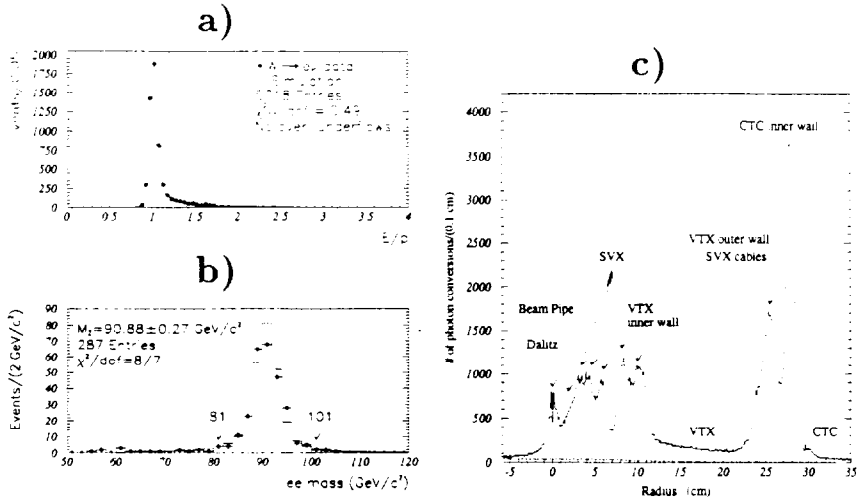

Figure 3: a) E/p distribution for $W \rightarrow e\nu$ events. The energy scale is obtained from a fit between 0.9 and 1.1 and the amount of material is obtained from a fit between 1.3 to 2.0. b) Mass distribution of $Z \rightarrow ee$ events. The constant term in the electron energy resolution is extracted from the width of this peak. c) Radial distribution of photon conversions to electron pairs. The main features of the CDF detector can be seen in this plot. The amount of material from E/p is checked using photon conversions which in the next measurement will be the primary source of material information.

the width of the $Z \rightarrow ee$ peak (Fig. 3b). It is parameterized as $\delta E/E = (13.5 \pm 0.7)\%/\sqrt{E_T} \oplus \kappa$ where the 13.5 ± 0.7 is obtained from test beam studies and κ is extracted from the $Z \rightarrow ee$ data and found to be $(1.0 \pm 1.0)\%$. The resolution uncertainties lead to an uncertainty in M_W of 80 MeV/c^2.

3.4 Neutrino Energy Calibration and Monte Carlo Simulation

Since the neutrinos from W decays are not detected, their transverse momentum is inferred by requiring momentum balance in the event. This relies on knowing the calorimeter response to the elements in the event other than the lepton. This calibration is done using $Z \rightarrow ee$ events where the transverse momentum of the Z is measured from the decay electrons and compared with the calorimeter measurement of the transverse recoil from the Z, $\vec{u} = \sum E_i \sin\theta_i \hat{\mathbf{n}}_i$, where the quantities are as defined in Sec. 2.1 (Fig. 4a).

Instead of attempting to parameterize the calorimeter response in Z events, the approach used here is to incorporate the $Z \rightarrow ee$ data itself in the W

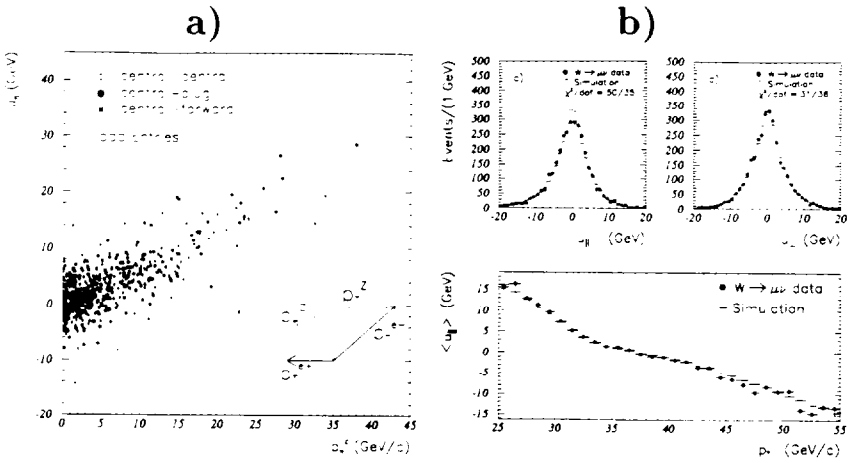

Figure 4: a) The systematic mismeasurement of the true recoil energy from the Z can be seen in this plot of $|\vec{u}|$ vs. p_T^Z. This information is used to calibrate the calorimeter response to the vector boson recoil. b) Distributions of $u_\parallel$ and $u_\perp$ (top) and $u_\parallel$ vs. p_T^μ (bottom) in $W \rightarrow \mu\nu$ data.

Monte Carlo simulation. The W Monte Carlo is a leading order generator plus parton distribution functions. The effect of NLO QCD is put in by hand in the form of an artificial p_T^W spectrum (constructed from the Z p_T spectrum) from which the LO decay leptons are boosted. The calorimeter response is modeled by choosing a Z event with the same p_T as the simulated W and using the calorimeter energy distribution from that event. This has the advantage of automatically including effects such as luminosity dependence (Z events arrive in constant proportion to W events). Using the Z data in this way leads to two uncertainties in M_W: that from the finite statistics of the Z sample and that from the intrinsic smearing of the electron-measured p_T^Z. Together they contribute a 60 MeV/c^2 uncertainty.

The two quantities of interest for comparing simulation to data are $u_\parallel$ and $u_\perp$ (Fig. 4b), which are the projections of $\vec{u}$ parallel and perpendicular to the lepton direction. The input p_T^W spectrum is constrained by the width of the $u_\perp$ distribution which is less sensitive to lepton energy removal than $u_\parallel$. The statistics of the $u_\perp$ distribution determine the uncertainty in the input p_T^W spectrum and together with a term from allowing the shape to vary contribute a 45 MeV/c^2 uncertainty in M_W.

The choice of parton distribution functions are constrained by the charge asymmetry of W decays (Fig. 5a). Because of the correlation between fitted

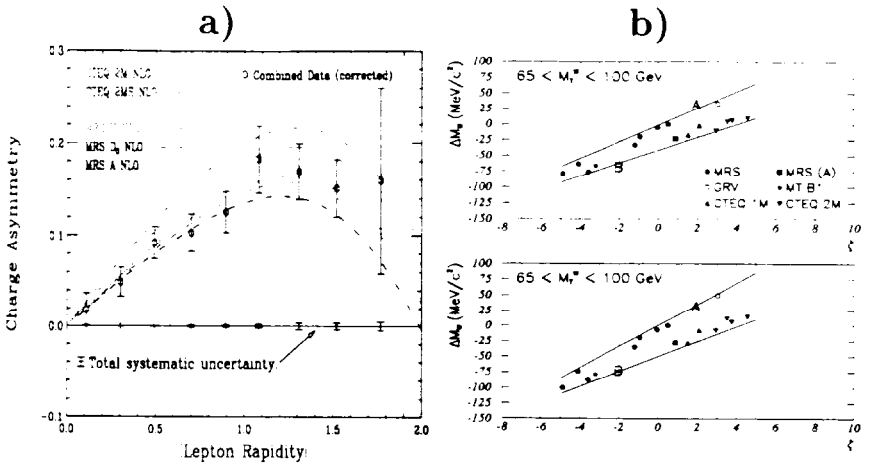

Figure 5: a) The charge asymmetry in W decays as a function of $|\eta|$. b) The fitted W mass as a function of deviation from CDF W asymmetry data for various parton distribution functions.

mass and asymmetry, a band of allowed parton distributions can be chosen in a quantitative fashion. This allowed band introduces an uncertainty of 50 MeV/c^2 into M_W.

As stated above, the simulation is a leading order generator with an uncorrelated p_T^W spectrum inserted by hand. The difference between this and NLO QCD is investigated using both a NLO QCD generator and a parameterization of the change in W polarization from NLO QCD. An uncertainty of 20 MeV/c^2 is attributed to these effects. Higher-order QED is incorporated by shifting the fitted mass value to account for radiative effects (65 MeV/c^2 for e and 168 MeV/c^2 for μ) and assigning an uncertainty of 20 MeV/c^2. This uncertainty is due to the fact that a complete QED radiative Monte Carlo did not exist for quark-antiquark W production and thus estimates were made based on several incomplete, but complementary, models.

The background processes (Fig. 6a) in the W mass samples are predominantly electroweak in nature. For electrons, the main background is $W \rightarrow \tau\nu \rightarrow e\nu\nu\nu$. This comprises 0.8% of the $W \rightarrow e\nu$ background and is included in the simulation. For muons, the dominant background is $Z \rightarrow \mu\mu$ where one muon goes undetected. This accounts for a 3.6% background in addition to the same τ background suffered by electrons. Again, both of these backgrounds are included in the simulation. The net effects are 10 MeV/c^2 and 25 MeV/c^2 uncertainties for $W \rightarrow e\nu$ and $W \rightarrow \mu\nu$ respectively.

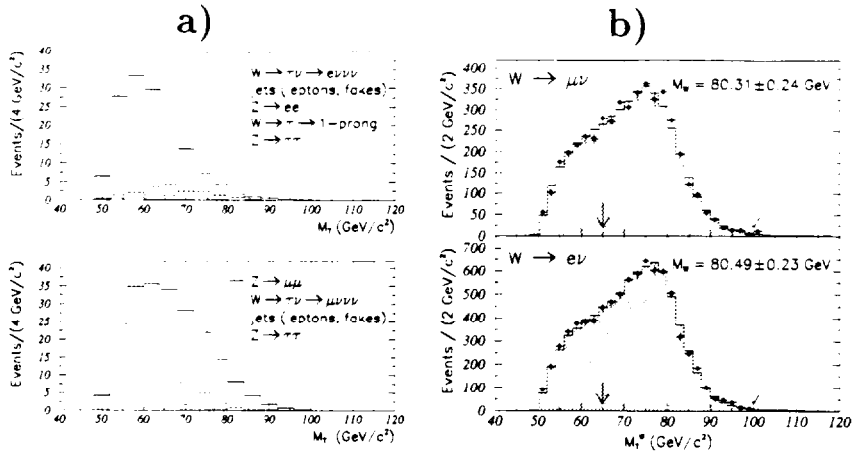

Figure 6: Backgrounds present in the $W \rightarrow e\nu$ sample (top) and $W \rightarrow \mu\nu$ sample (bottom). b) Transverse mass distributions for electrons (top) and muons (bottom). The uncertainty is statistical plus systematic.

Transverse mass lineshapes are generated at various values of M_W, and an unbinned likelihood for the data is calculated with each lineshape with the maximum likelihood giving the best fit mass. A plot of the transverse mass distributions for $W \rightarrow e\nu$ and $W \rightarrow \mu\nu$ with the best fit simulation histograms overlayed are shown in Fig. 6b. The statistical uncertainty of the fit is the mean uncertainty returned from the likelihood fit for simulated data samples of the same size as the $W \rightarrow e\nu$ and $W \rightarrow \mu\nu$ data samples. There is also a small fitting uncertainty of 10 MeV/c^2 caused by the finite number of simulated events in the fitting lineshapes.

3.5 Mass Values and Uncertainties

The fitted mass values are

$$M_W^e = 80.490 \pm 0.145(stat) \pm 0.175(syst) \text{ GeV/c}^2 \quad (3)$$

$$M_W^\mu = 80.310 \pm 0.205(stat) \pm 0.130(syst) \text{ GeV/c}^2. \quad (4)$$

Taking into account common uncertainties, these values combine to give

$$M_W^{e+\mu} = 80.41 \pm 0.18 \text{ GeV/c}^2. \quad (5)$$

The uncertainties in these numbers are listed in Table 4. Comparisons with

Table 4: Uncertainties in the W mass measurement for Run 1A and predictions for Run II.

RUN 1A — 20pb^{-1} Uncertainty in M_W	(MeV/c^2)			**RUN II — 1fb^{-1}** (MeV/c^2)		
	e	μ	Com	e	μ	Com
Statistical	**145**	**205**	—	**20**	**30**	—
Energy Scale	**120**	**50**	**50**	**30**	**20**	**20**
Scale from J/ψ	50	50	50	20	20	20
CTC Alignment	15	15	15	—	—	—
Calorimeter	110	—	—	25	—	—
Other Systematics	**130**	**120**	**90**	**40**	**40**	**35**
e or μ Resolution	80	60	—	10	10	—
Input p_T^W	45	45	25	10	10	10
Recoil Modeling	60	60	60	10	10	10
e or μ ID and Removal	25	10	5	10	5	5
Trigger Bias	0	25	—	0	10	—
Parton Dist. Functions	50	50	50	25	25	25
Radiative Corrections	20	20	20	10	10	10
W Width	20	20	20	10	10	10
Higher-order Corrections	20	20	20	10	10	10
Backgrounds	10	25	—	5	10	—
Fitting	10	10	—	10	10	—
Total Uncertainty	**230**	**240**	**100**	**54**	**54**	**40**

previous measurements are made in Fig. 7 along with implications for the higgs mass.

4 The Future

The CDF detector has just finished collecting 5 times more data than this paper is based on and analyses are underway to measure the cross sections and the W mass and width. The expected gain in the W mass uncertainty and in the W width direct measurement should be a factor of 2. In the long term, Fermilab's tevatron, with its newly installed Main Injector, is expected to start colliding again in late 1999 with the expectations of giving CDF and DØ over 1fb^{-1} each. Table 4 lists the expected uncertainties in the W mass from 1fb^{-1} of data. The statistical uncertainty for muons should be less than that quoted here because of a planned increase in muon chamber coverage. Most

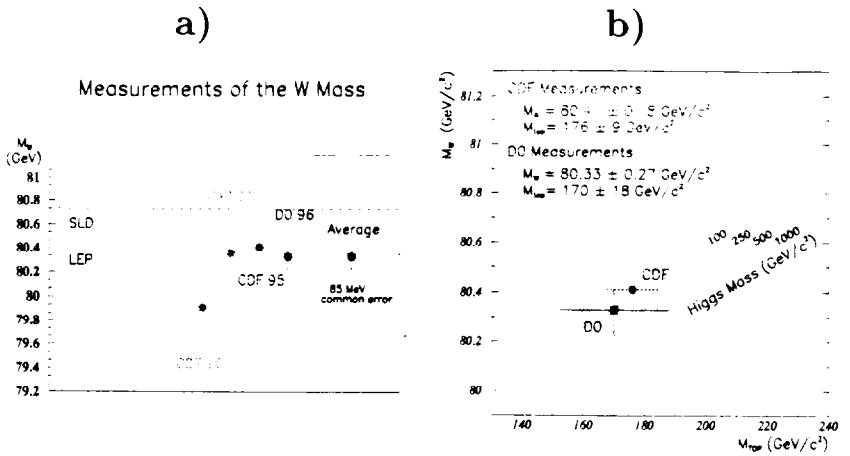

Figure 7: a) This and previous measurements of the W mass. b) Relationship between the W mass, the higgs mass and the top mass. The DØ numbers in both figures are from Run 1a. For a preliminary Run 1B DØ W mass number see the writeup by E. Flattum in these proceedings.

of the systematic uncertainties scale with number of events, but the change in the uncertainty from parton distribution functions is harder to quantify. It is however expected to decrease since it depends on the W charge asymmetry measurement (Fig. 8a). The higgs mass predicting power improves as expected and is shown in Fig. 8b including the expected top quark uncertainty.

Acknowledgments

We thank the Fermilab staff and the technical staffs of the participating institutions for their vital contributions. This work was supported by the U.S. Department of Energy and National Science Foundation; the Italian Instituto Nazionale de Fisica Nucleare; the Ministry of Education, Science and Culture of Japan; the Natural Sciences and Engineering Research Council of Canada; the National Science Council of the Republic of China; and the A.P. Sloan Foundation.

References

1. F. Abe *et. al.* (CDF Collaboration), *Phys. Rev. Lett.* **73**, 220 (1994). F. Abe *et. al.* (CDF Collaboration), *Phys. Rev.* D **52**, 2624 (1995). For

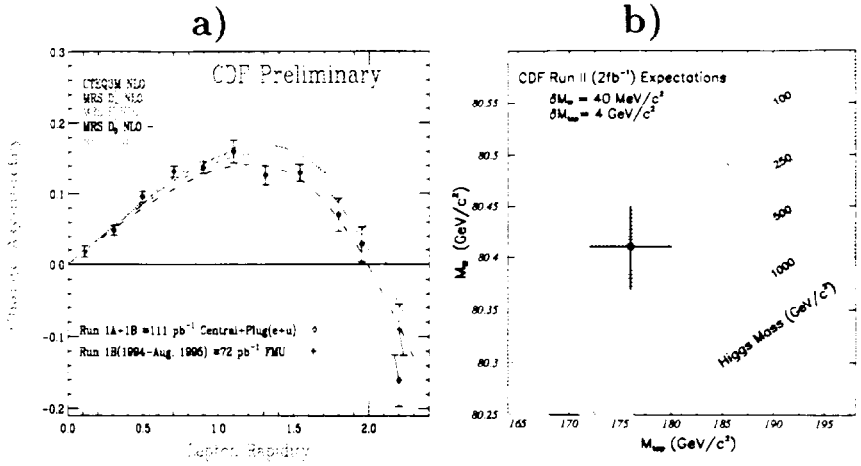

Figure 8: a) Preliminary Run 1B W charge asymmetry measurement. As this measurement gets better, the constraint on allowed parton distribution functions gets better. b) Relationship between the W mass, the higgs mass and the top mass for Run II with $2fb^{-1}$.

a discussion of the muon channel, see W.F.Badgett, The CDF Collaboration, *Proceedings of the Eighth Meeting of the Division of Particles and Fields of the American Physical Society (DPF'94)* , University of New Mexico, Albuquerque, NM, August 2-6, 1994.

2. F. Abe *et. al.* (CDF Collaboration), *Phys. Rev. Lett.* **74**, 11 (1994). F. Abe *et. al.* (CDF Collaboration), *Phys. Rev.* D **52**, 4784 (1995).
3. F. Abe *et. al.* (CDF Collaboration), *Phys. Rev. Lett.* **74**, 342 (1995).
4. All published CDF papers contain brief descriptions of the detector, for a more detailed discussion, see F. Abe *et. al.* (CDF Collaboration), Nucl. Instrum. Methods Phys. Res. A **271**, 387 (1988).
5. M. Aguilar-Benitez *et. al.* (PDG), *Review of Particle Properties* from *Phys. Rev.* D **45**, (1992); *Phys. Rev.* D **50**, (1994).